Advances in Aircraft and Spacecraft Science, *Vol. 3, No. 3 (2016) 259-269*
DOI: http://dx.doi.org/10.12989/aas.2016.3.3.259

Flow-induced interior noise from a turbulent boundary layer of a towed body

J. Abshagen*, D. Küter and V. Nejedl

Research Department for Underwater Acoustics and Marine Geophysics (FWG), Bundeswehr Technical Centre WTD 71, Berliner Straße 115, 24340 Eckernförde, Germany

(Received May 30, 2015, Revised September 22, 2015, Accepted October 3, 2015)

Abstract. In this work results from an underwater experiment on flow-induced noise in the interior of a towed body generated from a surrounding turbulent boundary layer are presented. The measurements were performed with a towed body under open sea conditions at towing depths below 100 m and towing speeds ranging from 2.4 m/s to 6.2 m/s (4 kn to 12 kn). Focus is given in the experiments to the relation between (outer) wall pressure fluctuations and the (inner) hydroacoustic near-field on the reverse side of a flat plate. The plate configuration consists of a sandwich structure with an (thick) outer polyurethane layer supported by an inner thin layer from fibre-reinforced plastics. Parameters of the turbulent boundary layer are estimated in order to analyse scaling relations of wall-pressure fluctuations, interior hydroacoustic noise, and the reduction of pressure fluctuations through the plate.

Keywords: interior flow noise; turbulent boundary layer; underwater experiment

1. Introduction

Turbulent pressure fluctuations are noise sources that can radiate into the far-field (Camussi 2013), but can also have impact as wall pressure fluctuations (Willmarth 1975, Farabee and Cassarella 1991) on the interior of a moving body due to a boundary layer flow (Schlichting 1965). In particular, the excitation of mechanical structures by turbulent wall pressure fluctuations provides a crucial mechanism of flow-noise generation (Blake 1986, Hambric 2004, De Rosa 2008, Ciappi 2013, Ciappi 2015). Interior flow-induced noise is of relevance, for instance, as cabin noise in automotive and aircraft applications (see e.g., Becker 2013, Hu 2013), but also in underwater systems (see e.g. Dowling 1998, Elboth 2012, Abshagen 2014). Here, flow-induced noise contributes to the so-called sonar self-noise which limits the hydroacoustic performance of a sonar system (Urick 1975).

Several open-sea experiments on flow-induced noise near the wall of underwater systems have been performed, for instance, with a towed body (Nishi 1969, Abshagen 2014), a lifting body (Galib 1994), and a towed array (Keith 2009, Elboth 2012). Hydrophones in the interior of a sonar system are often shielded by a mechanical structure which is entirely immersed into water. Suitable materials for a hull structure need to fulfil specific requirements with respect to stability,

*Corresponding author, Dr., E-mail: janabshagen@bundeswehr.org

http://www.techno-press.org/?journal=aas&subpage=7 ISSN: 2287-528X (Print), 2287-5271 (Online)

(a) FLAME towed body (b) sound speed profile

Fig. 1 (a) Picture of FLAME towed body with flat plate configuration (measurement area: white rectangle) during release from towing vessel RV ELISABETH MANN BORGESE, (b) sound velocity profile measured in Sognefjord, Norway, directly before the towing experiment

hydroacoustic performance, and vibroacoustic properties. Ideally such materials should be transparent to underwater far-field sound, but shield the flow-induced noise generated from the turbulent boundary layer.

In this work the behaviour in the hydroacoustic near-field on the reverse side of a submerged plate excited by an (outer) turbulent boundary layer flow is investigated. Particular focus is given to the relation between hydrodynamic wall pressure fluctuations and (interior) hydroacoustic pressure fluctuations. The plate configuration considered in this work consists of an (thick) outer layer made of polyurethane supported by an (thin) inner layer from fibre-reinforced plastics. Polyurethane has preferable hydroacoustic properties, because the impedance is close to that of water. The flat plate was laterally attached to a towed body designed for flow noise measurements and the towing experiments were performed under open sea conditions for different towing speeds at towing depths below 100 m.

2. Underwater experiments with towed body

The research cruise was performed with RV ELISABETH MANN BORGESE from the Institute of Baltic Sea Research (IOW), Germany, in the Sognefjord, Norway, in September 2014. The so-called FLAME (**FL**ow Noise **A**nalysis and **M**easurement **E**quipment) towed body measurement system used during this research cruise was designed by the company ATLAS Elektronik (Bremen, Germany) in cooperation with FWG for flow noise measurements under open sea conditions. The towed body has a length of 5.26 m, a width of 1.353 m (0.935 m without fins), and a total height of 1.715 m. The weight in air is about 2800 kg and the total mass of the body flooded with water amounts roughly 3500 kg. A picture of the FLAME towed body during release from the research vessel is shown in Fig. 1(a). The body was towed at a speed between U=2.4 m/s to 6.2 m/s (4 to 12 kn) below the local thermocline at depths of more than 100 m in order to reduce disturbing oceanic inflow turbulence. The sound velocity profile measured directly before the towing experiment in Sognefjord with the integrated CTD probe on-board RV ELISABETH MANN BORGESE is depicted in Fig. 1(b). The sound velocity profile is almost constant below 100 m. The distance between towing vessel and towed body was between 400 and 600 m in order to reduce hydroacoustic disturbances from the towing vessel. The GPS track of RV ELISABETH

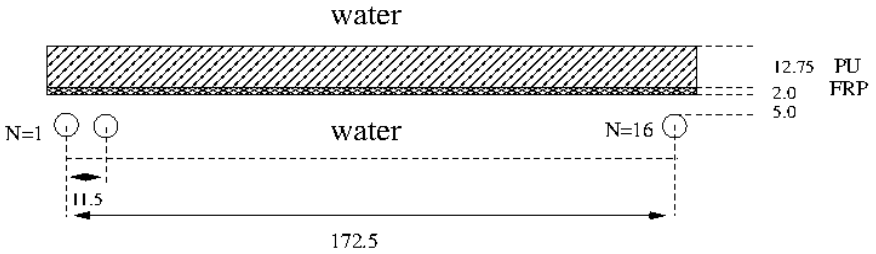

Fig. 2 Sandwich plate configuration of thick polyurethane (PU) layer supported on the inside by a thin fibre-reinforced plastic (FRP) layer and surrounded by water. The position of the hydrophones (N=1,...,16) in the interior of the towed body are given (unit of length in mm). Flow direction is from right to left

MANN BORGESE is recorded for each measurement run and the average speed over ground (SOG) is calculated as an estimated value for the average flow speed for each track. A single run typically requires 360 s of data recording time.

The measurement area within the flat plate region of the towed body is a rectangle of 300 x 575 mm in vertical and horizontal direction, respectively. It appears as a white rectangle inside of the (brown) plate in Fig. 1 (a). The white rectangle is made of a layer of polyurethane (PU) with a thickness of 12.75 mm that is supported by a layer of 2 mm thickness made of fibre-reinforced plastic (FRP) on the inner side of the towed body. Since the interior of the towed body is flooded, the sandwich structure is surrounded by water. The plate configuration can be seen in Fig. 2.

The measurement area is baffled by a steel plate which is covered by a hard foam from the outside (brown area in Fig. 1 (a)). The plate is not mounted flush to the towed body but it is elevated by 10 mm in wall normal direction. Leading and trailing edges of the plate are smoothed with an entrance length of 800 mm at the leading edge. Wall pressure fluctuations are measured with a RESON 4050 flush-mounted hydrophone (fmh), which is located on the horizontal centre line 65 mm downstream from the measurement rectangle within the steel plate baffle. The hydroacoustic noise in the interior is measured with an array of 16 RESON 4013 hydrophones, which are positioned with a spacing of 11.5 mm on the horizontal centre line behind the plate at a distance of 5 mm from the (inner) wall (Fig. 2). The hydrophone array is mechanically shielded from the internal structure of the towed body in order to reduce the impact of internal structural vibrations and hydroacoustic background noise. The rigid body motion of the towed body was stabilised before each measurement run by a motion control on-board RV ELISABETH MANN BORGESE to only a few degrees in pitch and roll. During data recording the towed body went on a straight track without further active control.

3. Results

3.1 Interior and exterior hydroacoustic noise

A wavenumber-frequency spectrum of the noise in the interior of the towed body, corresponding to the measurement at U=4.2 m/s is depicted in Fig. 3(a). The wavenumber-frequency spectrum and all power spectral densities (PSD) in this work are calculated with a bandwidth of Δf=1 Hz from an average over 360 short-time (Hamming windowed) 2-d and 1-d

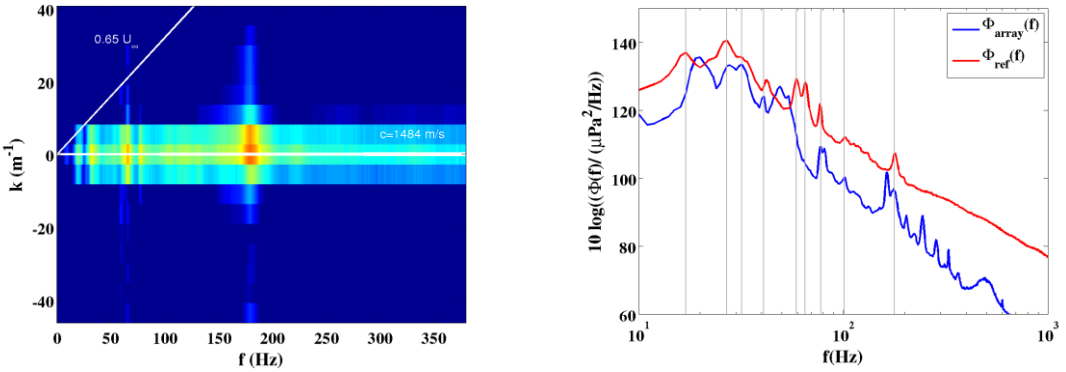

(a) wavenumber-frequency spectrum (b) power spectral density

Fig. 3 (a) Wavenumber-frequency spectrum of interior hydroacoustic noise (the speed of sound, c, and an approximate convective speed 0.65 U_∞ is indicated), (b) Power spectral densities of interior hydroacoustic noise, Φ_{array}, and of (averaged) hydroacoustic noise, Φ_{ref}, measured on the opposite side of the towed body with several reference hydrophones. Vertical lines correspond to peaks from external noise sources

Fast Fourier transforms, respectively. Because the spacing between the hydrophones is 11.5 mm, the maximum resolved wavenumber yields $k \approx \pm 40$ m^{-1} (due to spatial sampling). The speed of sound at towing depth and an approximate convective speed 0.65 U_∞ are indicated in the wavenumber-frequency spectrum. The acoustic length of the array is 184 mm and this limits the wavenumber resolution to $\Delta k = 5.4$ m^{-1}. Because of the large wavelengths of (hydroacoustic) sound in the considered frequency regime, the direction of underwater sound is not resolved in Fig. 3(a). It can be seen from Fig. 3(a) that other than hydroacoustic noise sources, such as the convective ridge of turbulent wall pressure fluctuations, do not contribute directly to the noise in the interior of the towed body. Non-acoustic sources would induce a significant spectral contribution at higher wavenumbers. Wavenumber-frequency analysis has been established as a powerful tool for investigations of the physical properties of flow-induced noise sources, which may reduce the performance of sonar antennas. Details of the method can be found in (Abshagen 2014).

The sea is a noisy environment and disturbances from external noise sources in free-field experiments need to be identified. Ambient noise induced from environmental sources, such as wind, waves, or rain, has generally a broadband character (Carey 2011) and is not masking the measurement signal in the low-frequency regime considered in this work. Spectral peaks resulting e.g., from the towing vessel, on the other hand, disturb the measurements in this regime. Several peaks which originate from external noise sources can be identified in the power spectral density Φ_{ref} shown in Fig. 3(b) (marked by vertical lines). Φ_{ref} is obtained from an average over several reference hydrophones located on the opposite side of the towed body (Abshagen 2014). Some of the peaks from external sources in Φ_{ref} can also be found in the power spectral density Φ_{array}, which is calculated from an averaged over all 16 array hydrophones in the interior of the towed body. Noise from external sources therefore contaminates the measurement.

3.2 Wall pressure fluctuations and interior hydroacoustic noise

The PSD of wall pressure fluctuations (Φ_{fmh}) and of interior hydroacoustic noise (Φ_{array}) is

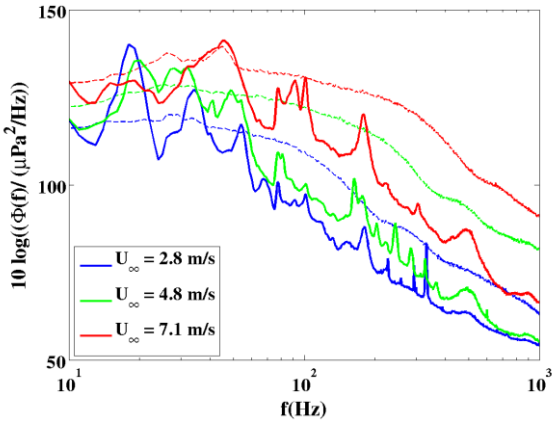

Fig. 4 Power spectral density (PSD) of wall pressure fluctuations Φ_{fmh} (dashed line) and interior hydroacoustic noise Φ_{array} (solid line) for three different towing speeds U=2.4 m/s, 4.1 m/s, and 6.2 m/s

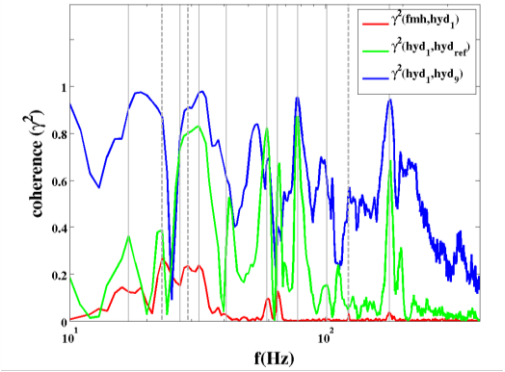

(a) coherence γ^2 between different positions

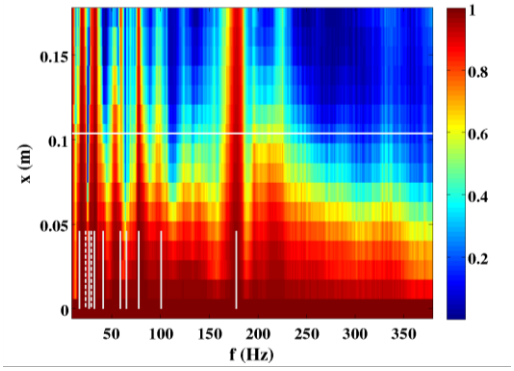

(b) spatial coherence $\gamma^2(f,x)$ along array

Fig. 5 (a) Coherence between interior noise measured with hyd1 and wall pressure fluctuations, $\gamma^2(fmh,hyd1)$, between interior noise and a references hydrophone on the opposite side, $\gamma^2(hyd1, hyd_{ref})$, and between two different positions along the array in the interior, $\gamma^2(hyd1, hyd9)$ of the towed body for U=4.2 m/s, (b) spatial coherence $\gamma^2(f,x)$ along the array in the interior of the towed body (the horizontal white line correspond to $\gamma^2(hyd1, hyd9)$). The vertical lines correspond to external source in (a) and Fig. 3(b)

shown in Fig. 4 for the three different towing speeds U= 2.4 m/s, 4.2 m/s, and 6.2 m/s. It can be seen that Φ_{array} contains several peaks for all towing speeds, whereas Φ_{fmh} generally displays a broadband behaviour. A substantial increase of spectral power with towing speed can be seen in Fig. 4, which is typical for both wall pressure fluctuation and interior noise. For each towing speed the spectral level of wall pressure fluctuations is in general significantly higher than that of interior hydroacoustic noise.

In Fig. 5(a) the (spatial) coherence γ^2 between wall pressure fluctuations and interior noise measured with a single hydrophone at position (1), i.e., $\gamma^2(fmh, hyd1)$, as well as between two hydrophones from the array, i.e., γ^2(hyd1, hyd9), is depicted for U=4.2 m/s. Furthermore the coherence between interior noise and underwater noise measured at the opposite side of the towed

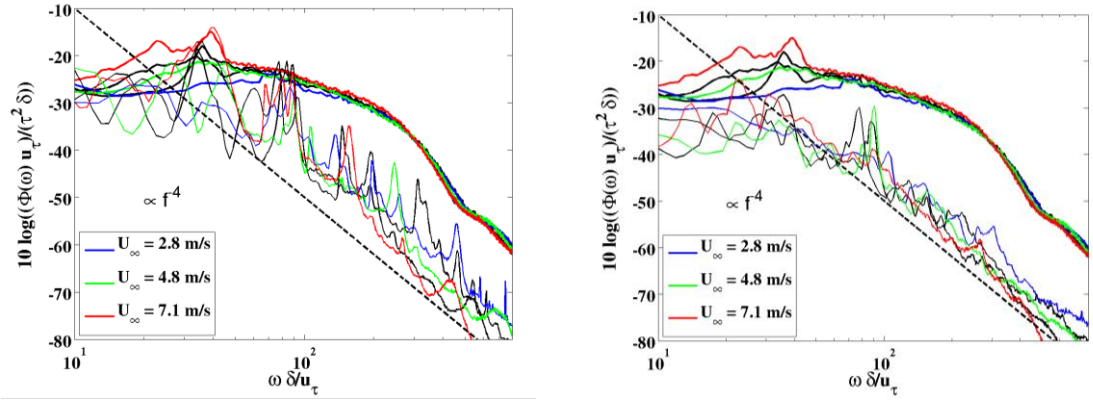

Fig. 6 Comparison of wall pressure fluctuations (Φ_{fmh}) with (a) hydroacoustic noise (Φ_{array}) and (b) incoherent hydroacoustic noise ($\Phi_{hyd1,inc}$) in the interior of the towed body. Pressure and time are scaled by boundary layer parameters. A f^{-4}-decay is shown for comparison

body with a single reference hydrophone, i.e., $\gamma^2(hyd1, hyd_{ref})$, is depicted. It can be seen that, though the level of coherence is generally lower, most of the peaks found in $\gamma^2(hyd1, hyd9)$ exist also in $\gamma^2(hyd1, hyd_{ref})$. This gives rise to external noise as the origin of spatial coherent signals. In Fig. 5(b) the spatial coherence $\gamma^2(x,f)$ along the array in the interior of the towed body is shown. $\gamma^2(x,f)$ is calculated from $\gamma^2(hyd1, hydN)$ (N=1,...,16). It can be seen from Fig. 5(b) that the frequency peaks of external noise sources, which are identified in Fig. 3(b) and 5(a), are characterized by large coherence lengths. This is a typical property of underwater sound in the frequency range considered here (Urick 1975).

Interior hydroacoustic noise, on the other hand, decays along the array and signatures from panel modes are not evident in the spatial coherence shown in Fig. 5(b). This allows a separation of (spatially coherent) external noise sources, e.g., of underwater sound, from (spatially incoherent) interior hydroacoustic noise. The (spatially) incoherent part of the PSD of interior hydroacoustic noise is calculated from $\Phi_{hyd1,inc}=\Phi_{hyd1}(1-\gamma^2(hyd1, hyd9))$. Φ_{hyd1} is the PSD obtained from measurements with a single hydrophone at position (1).

The flow field was not directly accessible in the experiments, but the outer flow velocity U_∞ and boundary layer quantities have been estimated from a two-dimensional potential flow around a symmetric body with semi-elliptical nose and tail having the same contour as the towed body at the vertical position of the hydrophones (the tail of the 2-*d* body was assumed to be identical to the nose for simplicity). The method is described in detail in (Abshagen 2015).

The potential flow U_∞ in arc-length coordinates is calculated from the *von Karman's* singularity method and from U_∞ the laminar momentum thickness Θ_{lam} is determined by *Thwaites'* method (Schlichting 1965, Cebeci 1999). This yields an estimation of the laminar boundary layer thickness and the displacement thickness under the assumption of flat plate conditions, i.e., $\delta_{lam}=5\ \Theta_{lam}/0.664$ and $\delta^*_{lam}=1.7208\ \Theta_{lam}/0.664$, respectively (Schlichting 1965). Laminar-turbulent transition in the boundary layer flow is determined from an extension of *Michel's* method (Cebeci 1999) and the turbulent boundary layer thickness δ is estimated from the flat plate relations (Schlichting 1965).

Table 1 Estimated values of boundary layer quantities. In brackets the values of the towing speeds U are given additionally in knots

U (m/s)	2.4 (4.7)	3.1 (6.1)	4.2 (8.1)	5.1 (9.9)	6.2 (12.0)
U_∞ (m/s)	2.8	3.6	4.8	5.9	7.1
u_τ (m/s)	0.098	0.125	0.163	0.196	0.234
δ (m)	0.0397	0.0377	0.0356	0.0339	0.0326
τ (N/m)	9.8	16.1	27.2	39.9	56.3

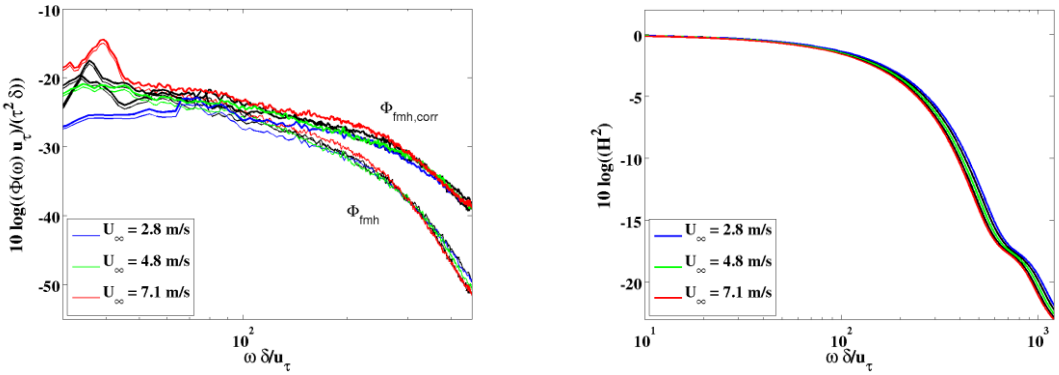

Fig. 7 (a) Power spectral density of wall pressure fluctuations scaled by boundary layer parameters with ($\Phi_{fmh,corr}$) and without (Φ_{fmh}) Corcos corrections. (b) Corcos correction H^2

Wall pressure fluctuations have been investigated at five different towing speeds U=2.4, 3.1, 4.2, 5.1, and 6.2 m/s. The estimated boundary layer quantities evaluated at the position of the flush-mounded hydrophone are given in Table 1.

A comparison of PSD of wall pressure fluctuations Φ_{fmh} with those of interior hydroacoustic noise Φ_{array} and of incoherent noise $\Phi_{hyd1,inc}$ is shown in Fig. 6 (a) and (b), respectively. Here, pressure and time are scaled by the estimated boundary layer parameters. It can be seen that the PSD of the wall pressure fluctuations Φ_{fmh} collapse onto each other in particular in the mid-frequency regime. Departures at lower frequencies result from disturbances, such as e.g., external noise, which are not related to the turbulent boundary layer flow. The collapse of the PSD of interior noise is in both cases not as good as for the wall pressure fluctuations, because a hydrodynamic scaling without any reference to the plate properties is used (Ciappi 2013). This can be seen in Fig. 6(a) for Φ_{array} and in (b) for $\Phi_{hyd1,inc}$. The spectral decay of $\Phi_{hyd1,inc}$, however, is much smoother in the mid- and high-frequency regime than that of Φ_{array}. The decay behaviour is close to a f^{-4}-law.

3.3 Corcos-correction of wall pressure PSD

In order to evaluate the reduction of pressure fluctuations through the plate the filtering of wall pressure fluctuations due to finite transducer size has to be determined (Corcos 1963, Lueptow 1995). For simplicity a Corcos correction with an assumed convective speed U_c=0.65 U_∞, an

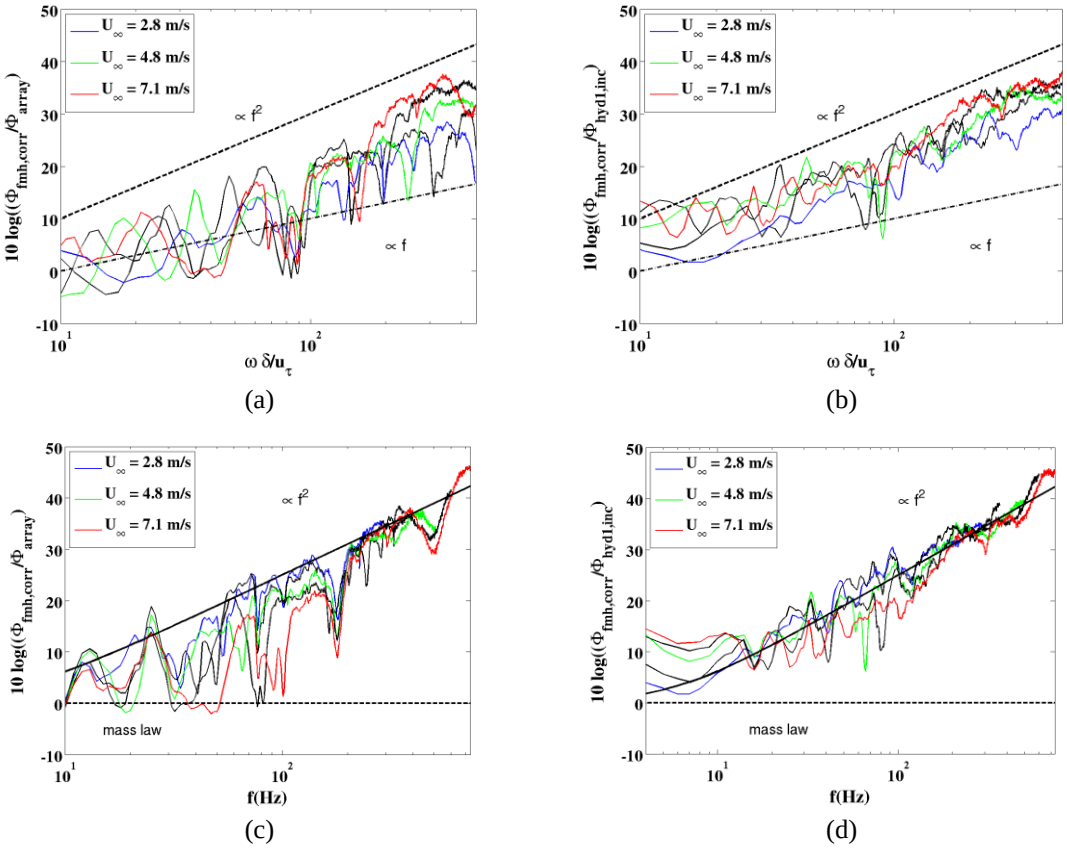

Fig. 8 Ratio between (Corcos-corrected) PSD of wall pressure fluctuations ($\Phi_{fmh,corr}$) and (a, c) interior hydroacoustic noise (Φ_{array}) or (b, d) incoherent noise ($\Phi_{hyd1,inc}$): (a, b) Dependence on normalized frequency $\omega\delta/u_\tau$ (dashed and dashed-dotted line correspond to a f^2 and a f^1-law, respectively) and (c,d) on the frequency f. A theoretical reduction index R_{wpf} (solid line) and the mass law for (incident) sound waves (dashed line) is plotted for comparison

effective transducer radius of r=4 mm, and Corcos parameters $\alpha_{1,3}$=0.7 and 0.11 in stream- and spanwise direction is applied. The scaled PSD of wall pressure fluctuations are depicted in Fig. 7(a) without (Φ_{fmh}) and with ($\Phi_{fmh,corr}$) Corcos correction. Here, the frequency interval is limited to a physically reasonable value at an upper bound. The Corcos correction H^2 is shown in Fig. 7(b) for different outer flow velocities. It can be seen that the filtering becomes relevant already for $\omega\delta/u_\tau > 10^2$.

3.4 Reduction index for pressure fluctuations

The transmission loss (TL) of an incident sound wave through a panel can be described by a *sound reduction index* $R_{sound}=10\log(1/\tau)$, where the transmission coefficient $\tau_{sound}=|p_T/p_I|^2$ is calculated from the ratio of pressure of transmitted (p_T) and incident (p_I) sound wave. In analogy to that, a transmission coefficient of wall pressure fluctuations through the panel can be defined by

the ratio of the PSD of interior hydroacoustic noise and wall pressure fluctuations, i.e., by $\tau_{wpf}=(\Phi_{array}/\Phi_{fmh,corr})$ or $\tau_{wpf,inc}=(\Phi_{hyd1,inc}/\Phi_{fmh,corr})$. Note, that here the outer pressure is not separated into an *incident* and a *reflected* part, as this is done for sound waves.

The reduction index R_{wpf} of wall pressure fluctuations found in the experiments is depicted in Fig. 8. In (a) and (b) R_{wpf} is plotted versus the normalized frequency $\omega\delta/u_\tau$, while in (c) and (d) the dependence on the frequency f is shown. In (a, c) the PSD of interior hydroacoustic noise Φ_{array} and in (b, d) the PSD of incoherent noise, i.e., $\Phi_{hyd1,\,inc,}$ is used. Corcos correction is applied to all PSD of wall pressure fluctuations, i.e., $\Phi_{fmh,corr}$ is used.

A significant increase of R_{wpf} by a f^{α}-law with an exponent α between α=1 and α=2 can be seen in all four cases. A f^2-behaviour is typical for the sound reduction index R_{sound}, if sound transmission is governed by the mass law, i.e., by $\tau_{sound}\approx 1/|1+i\,(\omega m/2\,\rho c)^2|$ (for normal incidence), with density of the medium ρ, sound speed c, mass of the panel (per unit area) m, and angular frequency ω. In order to illustrate the transmission behaviour of the panel for underwater sound the sound reduction index R_{sound} according to the mass law is plotted in Fig. 8 (c) and (d). Here, idealized values of the density for the polyurethane ($\rho=\rho_0$) layer of thickness 12.75 mm and the fibre-reinforced plastic layer ($\rho=2\rho_0$) of thickness 2 mm are assumed (Fig. 2). ρ_0 =1026 kg/m^3 is the density of sea water.

It can be seen from Fig. 8 (c, d) that according to the mass law the panel is almost transparent to (normal incident) underwater sound. In Fig. 8(c) several collapses of the measured reduction index $R_{wpf}\approx 0$ can be seen. This provides evidence that the behaviour of R_{wpf} is dominated by (external) underwater sound for those frequencies. The disturbances from external noise sources, such as underwater sound, is removed in (d) and the increase of R_{wpf} is much smoother. It basically follows a f^2-law, which suggests a mass-controlled process to be involved in the reduction of wall-pressure fluctuations. Considering a general transmission coefficient $\tau=1/|1+(Z/\rho_0\,c)^2|$, with plate impedance $Z=p/v$ (p pressure, v panel velocity), than Z would be three orders of magnitude larger for R_{wpf} than for R_{sound}. In Fig. 8 (c), (d) a curve with $Z=2500\ \omega$ m is plotted for comparison.

5. Conclusions

The specific environmental conditions (Carey 2011) at open sea make it necessary to evaluate the applicability and robustness of concepts gained from numerical and laboratory studies by underwater experiments. Towed body experiments on flow-induced noise are performed with RV ELISABETH MANN BORGESE in Sognefjord, Norway. The focus of the work was on the relation between wall pressure fluctuations and interior hydroacoustics noise in the presence of a solid wall structure having preferable hydroacoustics properties. In contrast to sound transmission, wall pressure fluctuations excite a wall structure of an underwater system typically at a much higher wavenumber than those of a sound wave at a comparable frequency. So, in general no coincidence between plate vibrations and wall pressure fluctuations can be expected for those systems.

Due to a coherence analysis the (spatially incoherent) interior hydroacoustic noise is separated from (spatially coherent) external sources, such as underwater sound. Evidence for a f^2-law in the reduction index of wall pressure fluctuations is found. The magnitude of the reduction index of wall pressure fluctuations, however, differs significantly from that of underwater sound for the

same frequency. This result is in general agreement with the transmission behaviour of panels for aircraft fuselage at much higher flow speeds (Orrenius 2009). The reduction of flow noise induced from a turbulent boundary layer by a mechanical structure along with hydroacoustic transparency is crucial in underwater applications.

Acknowledgments

The excellent support from the Technical Department of WTD71-FWG and ATLAS Elektronik as well as from Captain and Crew of RV ELISABETH MANN BORGESE is gratefully acknowledged.

References

Abshagen, J. and Nejedl, V. (2014), "Towed body measurements of flow noise from a turbulent boundary layer under sea conditions", *J. Acoust. Soc. Am.*, **135**, 637-645.

Abshagen, J., Schäfer, I., Will, Ch. and Pfister, G. (2015), "Coherent flow noise beneath a flat plate in a water tunnel experiment", *J. Sound Vib.*, **340** 211-220.

Blake, W.K. (1986), *Mechanics of flow-induced sound and vibration*, Academic Press, New York.

Camussi, R. (2013), *Noise sources in turbulent shear flow: fundamentals and applications*, CISM Courses and Lectures, Springer, Wien.

Carey, W.M. and Evans, R.B. (2011), *Ocean Ambient Noise: Measurement and Theory*, Springer, New York.

Cebeci, T. and Cousteix, J. (1999), *Modeling and computation of boundary-layer flows*, Horizons Publishing Inc., Long Beach, CA.

Ciappi, E., De Rosa, S., Franco, F., Guyader J.L. and Hambric, S.A. (2015), *Flinovia-Flow Induced Noise and Vibration Issues and Aspects*, Springer, Cham.

Ciappi, E., Magionesi, F., De Rosa, S. and Franco, F. (2013), "Analysis of the scaling laws for the turbulence driven panel responses", *J. Fluid. Struct*., **32**, 90-103.

Corcos, G.M. (1963), "Resolution of pressure in turbulence", *J. Acoust. Soc. Am*., **35**, 192-199.

De Rosa, S. and Franco, F. (2008), "Exact and numerical response of a plate under turbulent boundary layer excitation", *J. Fluid. Struct*., **24**, 212-230.

Dowling, A.P. (1998), "Underwater flow noise", *Theor. Comput. Fluid Dyn*., **10**, 135-153.

Elboth, T., Reif, B.A., Andreassen, Ø. and Martell, M.B. (2012), "Flow noise reduction from superhydrophobic surfaces", *Geophys.*, **77**, P1-P10.

Farabee, T.M. and Casarella, M.J. (1991), "Spectral features of wall pressure fluctuations beneath turbulent boundary layers", *Phys. Fluid. A*, **10**, 2410-2420.

Galib, T.A., Katz, R.A., Ko, S.H. and Sandman, B. (1994), "Measurements of turbulent pressure fluctuations using a buoyant vehicle coated with a thin elastomer layer", *J. Acoust. Soc. Am*., **96**, 3800-3803.

Hambric, S.A., Hwang, Y.F. and Bonness, W.K. (2004), "Vibration of plates with clamped and free edges excited by low-speed turbulent boundary layer", *J. Fluid. Struct*., **19**, 93-110.

Hu, N., Buchholz, H., Herr, M., Spehr, C. and Haxter, S. (2013) "Contribution of different aeroacoustic sources to aircraft cabin noise", *19th AIAA/CEAS Conference*, DOI: 10.2514/6.2013-2030.

Keith, W.L, Cipolla, K.M. and Furey, D. (2009), "Turbulent wall pressure fluctuation measurements on a towed model at high Reynolds numbers", *Exp. Fluid.*, **46**, 181-189.

Lueptow, R.M. (1995), "Transducer resolution and the turbulent wall pressure spectrum", *J. Acoust. Soc. Am*., **97**, 370-378.

Müller, S., Becker, S., Gabriel, Ch., Lerch, R. and Ulrich, F. (2013), "Flow-induced input of sound to the interior of a simplified car model depending on various setup parameters", *19th AIAA/CEAS Conference*, DOI: 10.2514/6.2013-2019.

Nishi, R.Y., Stockhausen, J.H. and Evensen, E. (1969), "Measurements of noise on an underwater towed body", *J. Acoust. Soc. Am.*, **48**, 753-758.

Orrenius, U., Cotoni, V. and Wareing, A. (2009), "Analysis of sound transmission through aircraft fuselages excited turbulent boundary layer or diffusive acoustic pressure fields", *Proc. 38th InterNoise Congress*, Ottawa, Canada, August.

Schlichting, H. (1965), *Grenzschicht-Theorie (Boundary Layer Theory)*, G. Braun, Karlsruhe.

Urick, R.J. (1975), *Principles of Underwater Sound*, 2nd Edition, McGraw-Hill, New York.

Willmarth, W.W. (1975), "Pressure fluctuations beneath turbulent boundary layers", *Annu. Rev. Fluid Mech*., **7**, 13-38.